LAWRENCE
LIVERMORE
NATIONAL
LABORATORY

LLNL-PROC-425667

Probing the isothermal (delta)->(alpha)' martensitic transformation in Pu-Ga with in situ x-ray diffraction

J. R. Jeffries, K. J. M. Blobaum, A. J. Schwartz, H. Cynn, W. Yang, W. J. Evans

March 12, 2010

MRS 2010 Spring Meeting: Actinides Symposium
San Francisco, CA, United States
April 5, 2010 through April 9, 2010

Disclaimer

Probing the isothermal δ→α′ martensitic transformation in Pu-Ga with in situ x-ray diffraction

Jason R. Jeffries,[1]Kerri J. M. Blobaum,[1] Adam J. Schwartz,[1] Hyunchae Cynn,[1] Wenge Yang,[2] and William J. Evans[1]
[1]Condensed Matter and Materials Division, Lawrence Livermore National Laboratory, Livermore, CA 94550, U.S.A.
[2]HPCAT, Advanced Photon Source, Argonne National Laboratory, Argonne, IL 60439, U.S.A.

ABSTRACT

The time-temperature-transformation (TTT) curve for the δ → α′ isothermal martensitic transformation in a Pu-1.9 at. % Ga alloy is peculiar because it is reported to have a double-C curve. Recent work suggests that an ambient temperature conditioning treatment enables the lower-C curve. However, the mechanisms responsible for the double-C are still not fully understood. When the δ → α′ transformation is induced by pressure, an intermediate γ′ phase is observed in some alloys. It has been suggested that transformation at upper-C temperatures may proceed via this intermediate phase, while lower-C transformation progresses directly from δ to α′. To investigate the possibility of thermally induced transformation via the intermediate γ′ phase, *in situ* x-ray diffraction at the Advanced Photon Source was performed. Using transmission x-ray diffraction, the δ → α′ transformation was observed in samples as thin at 30 μm as a function of time and temperature. The intermediate γ′ phase was not observed at -120°C (upper-C curve) or -155°C (lower-C curve). Results indicate that the bulk of the α′ phase forms relatively rapidly at -120°C and -155 °C.

INTRODUCTION

In a Pu-1.9 at.% Ga alloy, the transformation from the metastable face-centered-cubic (fcc) δ phase to the metastable, monoclinic α′ phase occurs via an isothermal (thermally induced) martensitic transformation at sub-ambient temperature [1]. A characteristic "C" shape is produced on a time-temperature-transformation (TTT) diagram—a contour plot showing the amount of transformation as a function of both time and temperature—due to the competition between driving and inhibiting forces controlling the transformation. In a Pu-1.9 at.% Ga alloy, the incomplete δ → α′ transformation exhibits anomalous double-C behavior, showing two temperatures at which the transformation proceeds in a minimal amount of time [2, 3]. While the Pu-1.9 at.% Ga alloy does not constitute the sole example of double-C kinetics in isothermal martensitic transformations, the observation of double-C phenomena in TTT diagrams is nonetheless rare [4, 5]. As such, Pu-Ga alloys provide an important test bed for understanding the competing forces and mechanisms that can drive double-C kinetics.

Previous reports suggest that the upper- and lower-C of the double-C curve can proceed through different mechanisms [6], and it has been speculated that the nucleation of α-Pu nuclei at room-temperature induces the lower-C [7-9]. Theoretical work suggests that the δ → α′ transformation must proceed through intermediate phases along the transformation path [10], and

pressure-dependent x-ray diffraction measurements of Pu-Am and Pu-Ga alloys have both revealed the presence of an intermediate γ' phase on the path to the pressure-induced α' phase [11, 12]. Herein, we report the results of an x-ray diffraction study at low temperature probing the kinetics of the thermally induced $\delta \rightarrow \alpha'$ transformation.

EXPERIMENTAL DETAILS

Two 3-mm diameter specimens of Pu-1.9 at.% Ga were used in these experiments: one disc-shaped sample was approximately 90 μm thick, while the other was approximately 30 μm thick. The samples were prepared using previously published techniques. In order to ensure that excess strains were not present, both samples were annealed at 375 °C for 8 hours and cooled to room temperature before being loaded into the sample holders [13]. The samples were affixed to the specimen mount of the sample holder with a small amount of Apiezon N-grease. A small amount of Cu powder was sprinkled on the samples in order to calibrate the detector-sample distance during cooling and isothermal holds at low temperature.

The sample holders were designed to triply encapsulate our radioactive materials, and simultaneously provide a large angular aperture for collection diffraction patterns. The sample holder comprised two main components: an oxygen-free high conductivity copper specimen mount, which housed the primary radiological seal, and an aluminum frame, which housed the secondary and tertiary radiological seals (see Fig. 1). The primary radiological seal was

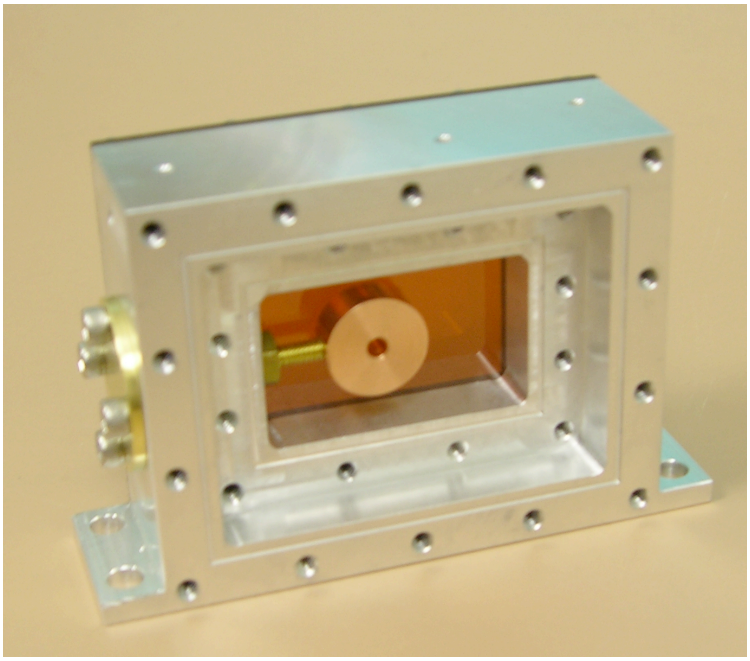

Figure 1. A photo of the triply encapsulated sample holder with only one side of seals assembled. The specimen mount is seen in the center of the aluminum frame. The sample rests in a small well that is countersunk into the central hole, which provides an aperture for the incident x-ray beam. O-ring grooves for indium o-rings are seen on the aluminum frame, which houses a nested design for the secondary and tertiary seals. Mylar and Kapton windows are used to minimize the attenuation of the incident and diffracted x-ray beams.

accomplished by attaching a 1-mil Mylar window, chosen for its small x-ray absorption in the hard x-ray regime, to the specimen mount using silicone. A brass retaining flange was used to support the Mylar window and prevent any loss of adhesion between the Mylar window and the specimen mount. The secondary and tertiary radiological seals were made of 1-mil thick, laser-cut Kapton windows. Grooves cut into the aluminum frame were filled with indium o-rings. The Kapton windows were forced into the indium o-rings by steel flanges secured with size 4-40 screws. The silicone-based primary seal combined with the secondary and tertiary compressed-indium seals provided hermetic seals that were leak-tight to helium (the Mylar and Kapton windows themselves have a non-zero permeability to He).

The triply encapsulated sample holder was mounted in a flow cryostat with liquid nitrogen used as the cryogen. Temperature was measured with a silicon diode thermometer mounted inside the aluminum frame of the sample holder. The temperature was controlled with a 100-watt heater in conjunction with a Lakeshore LS-340 temperature controller. The cryostat achieved cooling rates greater than 10 °C/min. down to approximately -120 °C; cooling rates down to -155 °C were greater than 5 °C/min.

Angle-dispersive x-ray diffraction (ADXD) patterns were acquired at the HPCAT beamline 16 BM-D of the Advanced Photon Source at Argonne National Laboratory. The x-ray beam, with an incident energy of 33 keV (λ_{inc} = 0.375 Å), was calibrated with CeO_2 and focused to 90 x 90 μm square spot. The energy of the beam permitted acquisition of diffraction patterns in a transmission geometry and the size of the beam allowed the beam to impinge upon multiple grains. Additionally, the specimens were rastered within the beam to sample as many grains as possible and provide diffraction patterns as close as possible to those of an expected powder pattern. The diffracted x-rays were detected with a Mar SX-165 CCD detector, which was capable of acquiring a diffraction pattern in 8 second intervals. The 2D diffraction patterns were collapsed onto a 1D intensity versus 2-Θ plot using the program FIT2D [14].

RESULTS AND DISCUSSION

The effects of the δ → α' transformation on the δ-matrix

Figures 2 and 3 show the results of x-ray diffraction patterns acquired after various isothermal hold times at -120 °C and -155 °C. The patterns have been normalized to the peak intensity of the (111) Bragg reflection of δ-Pu. The prominent Bragg reflections, including those of the Cu distance marker, are labeled in the topmost diffraction pattern of Figure 2(a) and 3(a). In all the diffraction patterns of Figure 2(a), the intensity of the (200) Bragg reflection of δ-Pu is greater than that of the (111) reflection. This is evidence of texturing in the specimen. On the contrary, the diffraction patterns corresponding to isothermal holds at -155 °C show very little texturing.

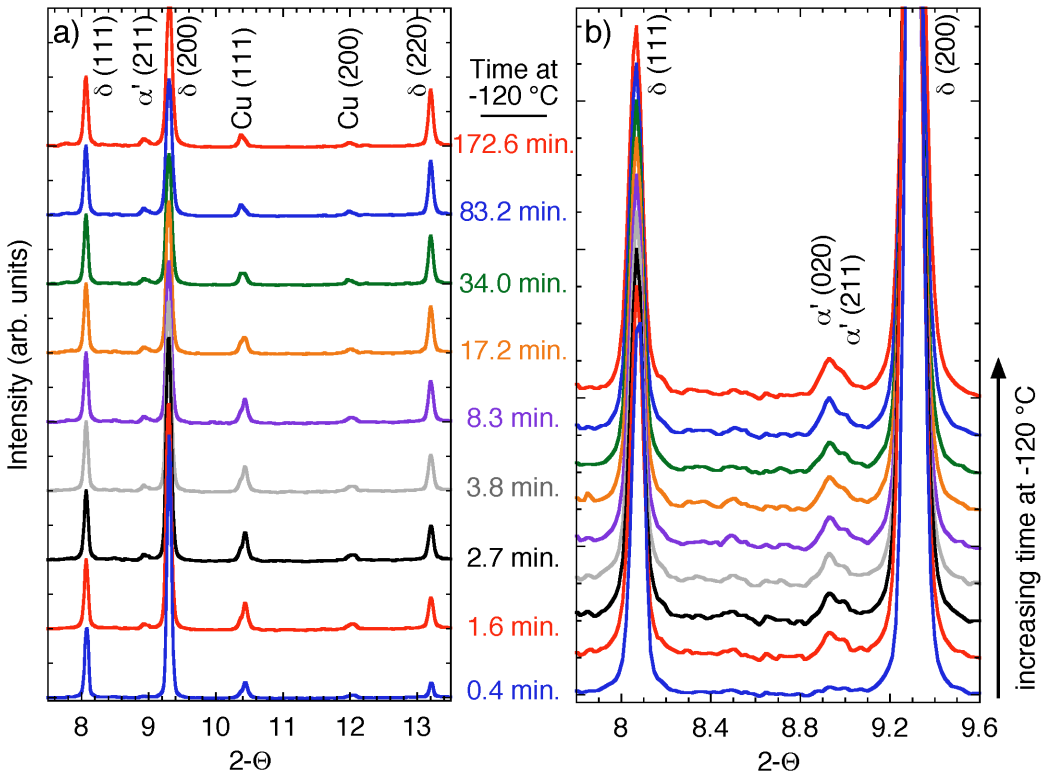

Figure 2. (a) Representative x-ray diffraction patterns of Pu-1.9 at.% Ga for various isothermal hold times at -120 °C. Diffraction patterns have been normalized to the peak intensity of the (111) Bragg reflection of δ-Pu. In addition to those of the Pu sample, there are Bragg peaks from the Cu distance marker located on the sample. (b) An expanded view of (a) illuminating the formation of the α′ phase, which is evinced by the increasing intensity of the (020)/(211) reflections with respect to the (111) reflection of δ-Pu . The order of the patterns of (b) is identical to that of (a).

There is no evidence in the diffraction patterns, even at the highest hold times, of any other intermediate phases, for instance, γ′. However, as shown in Figure 4, the patterns taken at -155 °C reveal a satellite peak that forms near the δ-phase (111) Bragg peak for long hold times. The (111) δ-phase reflection moves to slightly lower 2-Θ, perhaps suggesting an expansion of the underlying, but strained, δ-matrix. The satellite peak, on the other hand, shifts to higher 2-Θ, separating from the (111) reflection with increasing hold time at -155 °C. After the sample is warmed back to room temperature, the satellite peak is no longer evident. Because no such satellite peak is observed for isothermal holds at -120 °C, it is possible that the satellite is a manifestation of the transformation mechanism at -155 °C, within the lower-C of the TTT diagram. More work is needed to clarify this possibility, as the cooling rates used in this study could have elicited transformation in the upper-C before the target temperature (in the lower-C) was reached.

The time-dependent formation of the α′ phase is evident from the increasing intensity of the α′ (020) and (211) Bragg peaks of Figures 2 and 3 with increasing hold time. Concomitant with the formation of the α′ phase, the Bragg peaks of the δ phase broaden and shift to lower 2-Θ. While the former is likely a consequence of the accumulation of strain—which has the tendency to broaden the peaks—within the δ-matrix, the latter indicates an expansion of the fcc δ-lattice. The lattice parameters calculated from the diffraction data at -120 °C and -155 °C are shown in Figure 5. While the fcc δ lattice expands slightly during the δ → α′ transformation at -120 °C, amounting to an expansion of about 0.2% after 90 minutes, the expansion incurred during the transformation at -155 °C is nearly twice as large, amounting to an expansion of approximately 0.35% after nearly 80 minutes. The disparate time-dependent expansion of the lattice parameters in the upper- and lower-C of the TTT diagram for Pu-1.9 at.% Ga may provide clues as to the mechanisms at work in this transformation. While the morphology of the α′ product phase formed in the upper- and lower-C appear identical [8], the kinetics of the transformation are more rapid in the latter. Could the rapid kinetics of the transformation in the lower-C "freeze" in more dislocations than the transformation in the upper-C, thus expanding the δ-matrix more during the lower temperature transformation? Understanding whether these observations are

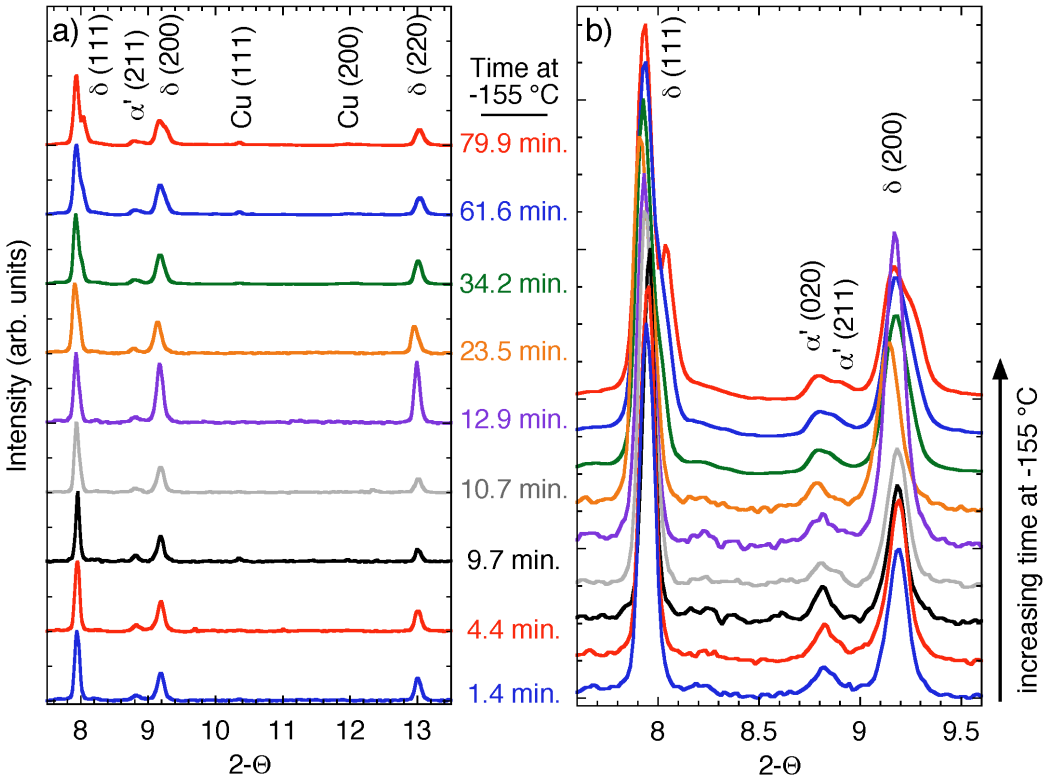

Figure 3. (a) Representative x-ray diffraction patterns of Pu-1.9 at.% Ga for various isothermal hold times at -155 °C. (b) An expanded view of (a) illuminating the formation of the α′ phase and the appearance of a satellite reflection associated with the (111) Bragg peak of δ-Pu. The order of the patterns of (b) is identical to that of (a).

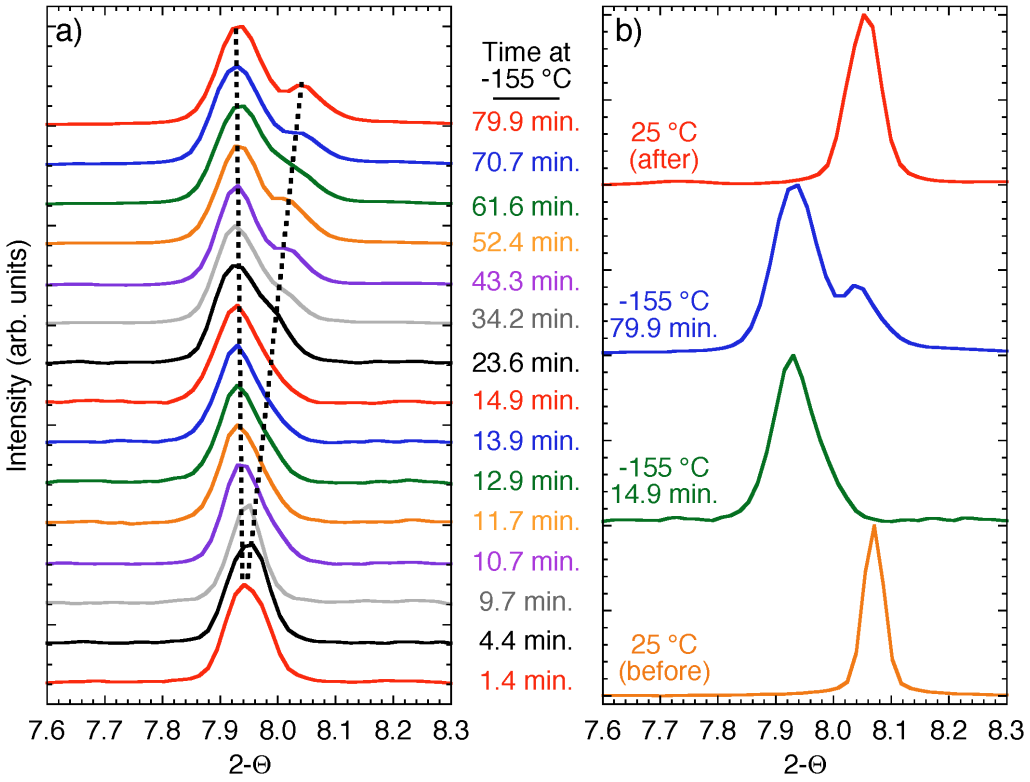

Figure 4. (a) The evolution of the (111) δ-Pu Bragg peak for hold times at -155 °C reveals a slight expansion of the δ lattice, strain-induced peak broadening, and the appearance of a satellite peak at high hold times. Dashed lines are guides to the eye. (b) That satellite peak separates from the (111) peak with increasing hold time; but, after the sample is warmed, the satellite peak disappears, leaving a (111) reflection characterizing increased strain in a slightly expanded δ-matrix.

results of the transformation kinetics or hallmarks of the transformation mechanisms has important consequences to our understanding of the $\delta \rightarrow \alpha'$ transformation in generl. The d-spacing corresponding to the (111) satellite peak seen in the diffraction patterns from isothermal holds at -155 °C is also shown in Figure 5. The satellite peak exhibits a contraction in d-spacing of nearly 1% after about 80 minutes at -155 °C. The nature of this satellite peak and its relation to the $\delta \rightarrow \alpha'$ transformation in the lower-C are still open questions.

The kinetic formation of α'

It can be seen in Figures 2 and 3 that a significant amount of the α' phase forms in as little as 1.6 minutes at -120 °C and 1.4 minutes at -155 °C. The amount of α' product phase formed can be estimated from the intensities of the Bragg reflections. The integrated intensity of a given Bragg reflection with indices hkl, I_p^{hkl}, is given by:

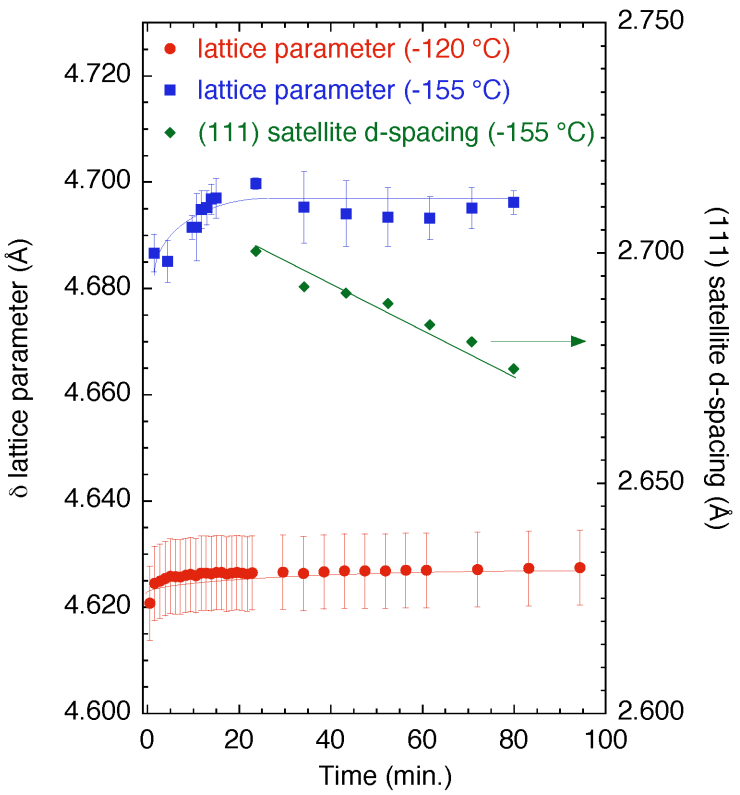

Figure 5. The evolution of the lattice parameters of the δ-matrix with isothermal holds at -120 °C and -155 °C as well as the d-spacing of the (111) satellite peak seen in the diffraction data at -155 °C. The lines are guides to the eye. There is a subtle expansion of the matrix at -120 °C, but the transformation at -155 °C seems to reveal a more dramatic expansion.

$$I_p^{hkl} = \frac{CV_p LP(\theta) M_p^{hkl} \left| F_p^{hkl} \right|^2 e^{-2W_p^{hkl}}}{v_p^2}, \qquad (1)$$

where C is an experimental constant, V_p is the volume fraction of a phase p, LP(θ) is the Lorentz polarization correction, M_p^{hkl} is the multiplicity of a Bragg reflection with indices hkl, F_p^{hkl} is the structure factor, W_p^{hkl} is the Debye-Waller factor evaluated at a d-spacing corresponding to an hkl Bragg reflection, and v_p is the unit cell volume. The combination of the vertical polarization and integration of the two-dimensional diffraction pattern resulted in a 2θ–independent Lorentz polarization correction. Structure factors were obtained from the Powdercell program. Debye-Waller factors were assumed to be isotropic, and were calculated according to Lawson et al. [15] and Baskes et al [16]. The unit cell volume was calculated from the positions of the Bragg peaks for the δ and α phases.

The alpha-prime volume fraction is calculated from the ratio of the intensities of the $(020)_\alpha$, $(211)_\alpha$, and $(111)_\delta$ Bragg reflections. The habit plane of the martensitic alpha-prime phase is $(020)_\alpha$ is parallel to $(111)_\delta$ [17]. By using these two Bragg reflections to calculate the alpha-prime volume fraction, errors associated with texturing are minimized. The $(020)_\alpha$ and $(211)_\alpha$ peaks could not be resolved as two distinct peaks due to the 2-theta resolution, so the measured integrated intensity was equal to the sum of the $(020)_\alpha$ and $(211)_\alpha$ Bragg reflections.

For simplicity, we let:

$$K_p^{hkl} = M_p^{hkl}\left|F_p^{hkl}\right|^2 e^{-2W_p^{hkl}}, \tag{2}$$

and let I_M equal the measured integrated intensity ratio such that:

$$I_M = \frac{I_\alpha^{020} + I_\alpha^{211}}{I_\delta^{111}} = \left(\frac{V_\alpha}{V_\delta}\right)\left(\frac{v_\delta^2}{v_\alpha^2}\right)\left(\frac{K_\alpha^{020} + K_\alpha^{211}}{K_\delta^{111}}\right). \tag{3}$$

Rearranging and solving for V_δ, with V_α=1-V_δ, yields:

$$V_\delta = \frac{v_\delta^2\left(K_\alpha^{020} + K_\alpha^{211}\right)}{I_M v_\alpha^2 K_\delta^{111} + v_\delta^2\left(K_\alpha^{020} + K_\alpha^{211}\right)}. \tag{4}$$

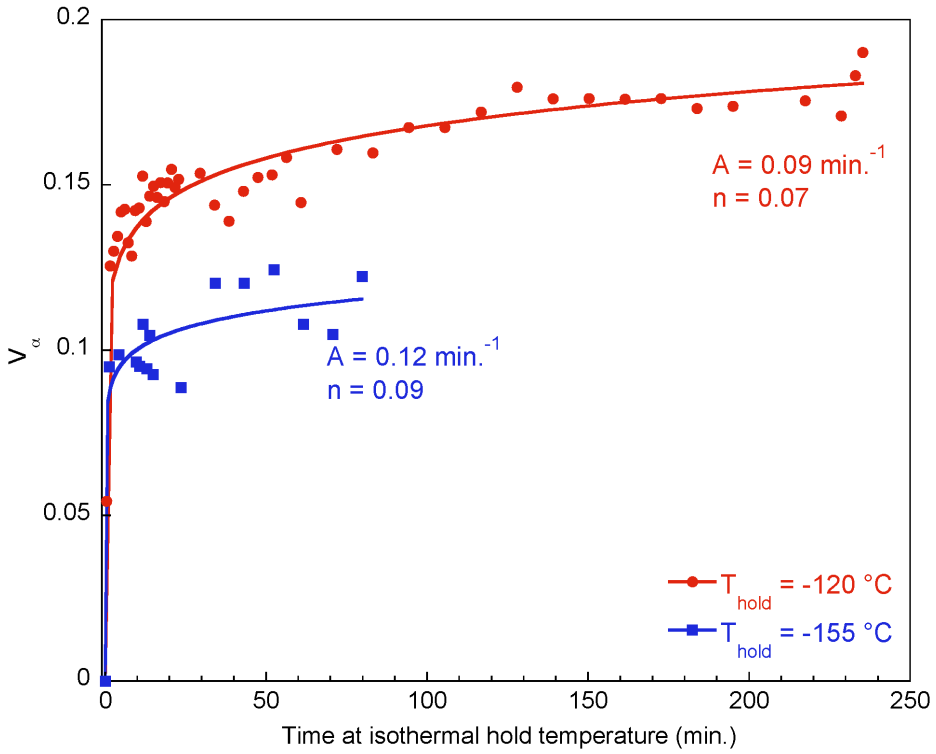

Figure 6. The volume fraction of α′ formed as a function of isothermal hold time at -120 °C and -155 °C. The solid lines are fits to a parameterized JMAK nucleation and growth formula (see text); the values of n from the JMAK formula are given next to each volume fraction curve.

The results of applying the above formulation to the diffraction patterns of Figures 2 and 3 are shown in Figure 6. The value of V_α for both isothermal hold temperatures exhibits a rapid onset with increasing hold time, followed by a much more gradual formation for times in excess of about 20 minutes. The values for the data at -155 °C exhibit more spread due to the presence of the satellite peak in the diffraction data at that temperature, which introduces uncertainty into the contribution of the (111) Bragg reflection intensity. The kinetics for both temperatures are comparable, although previous microstructural evidence suggests that the α′ phase forms more rapidly in the lower-C [8].

The time dependence of the α′ volume fraction is fit with a parameterized, kinetic Johnson-Mehl-Avrami-Kolmogorov (JMAK) nucleation and growth model [18-22]:

$$V_\alpha(t) = 1 - \exp(-At^n), \tag{5}$$

where A describes the time rate of change of the product of nucleation and growth of the forming α′ particles and n is related to the specific time dependence of the growth and nucleation rates. For constant nucleation and growth in three unconstrained dimensions, n=4. A smaller value of n represents a more rapid formation, via the *product* of nucleation and growth, of the product phase. While the values of n and A determined from the fits to the data shown in Figure 6 are small, owing to the rapid formation of α′-Pu at low times, these values are comparable to those reported by Ravat et al [23].

Interpretations of the fundamental underpinnings of such a small value for n are difficult. The morphology of α′ particles forming in the δ-matrix is acicular, with the α′ particles forming in long, thin plate-like or lenticular microstructures. While the particles are undoubtedly three-dimensional, the morphology of the microstructure would suggest that there exist constraints along certain crystallographic directions. This microstructure might suggest a reduced value of n in the JMAK formula, but low effective dimensionality alone cannot account for the values of n<1. If the progenitor nuclei for the α′ product phase are preformed, which has been previously suggested by the authors, then the nucleation kinetics become irrelevant within the construct of the JMAK formula, leading to a reduction in the value for n. The observed change in the lattice parameter of the δ-matrix may also play a role in determining the kinetics of the transformation as strains from the large δ/α′ volume discrepancy accumulate. There appears to be compounding and complicated effects driving the kinetics of the δ → α′ transformation.

SUMMARY

Angle-dispersive x-ray diffraction measurements probing the δ → α′ transformation have been performed on Pu-1.9at.% Ga specimens in situ at -120 °C and -155 °C. The transformation expands the δ-matrix, with the expansion being greater at -155 °C than at -120 °C. A satellite structure is observed in the data at -155 °C, but absent in the diffraction data at -120 °C. At these temperatures, the α′ product phase forms rapidly, and can be characterized by a JMAK nucleation and growth formula. The results of applying the JMAK formula are consistent with previous reports of the δ → α′ transformation at -130 °C, but interpreting the fundamentals

governing the values of the JMAK constants (A and n) remains a challenging questions with many possible scenarios.

ACKNOWLEDGMENTS

Lawrence Livermore National Laboratory is operated by Lawrence Livermore National Security, LLC, for the U.S. Department of Energy, National Nuclear Security Administration under Contract DE-AC52-07NA27344. This work was performed at HPCAT (Sector 16), Advanced Photon Source (APS), Argonne National Laboratory. HPCAT is supported by DOE-BES, DOE-NNSA, NSF, and the W.M. Keck Foundation. APS is supported by DOE-BES, under Contract No. DE-AC02-06CH11357.

REFERENCES

1) S. S. Hecker, D. R. Harbur, and T. G. Zocco, Prog. Mater. Sci. **49**, 429 (2004).
2) J. T. Orme, M. E. Faiers, and B. J. Ward, in *Plutonium 1975 and Other Actinides*, edited by H. Blank and R. Lindner (North Holland, Amsterdam, 1976), p 761.
3) B. Oudot, K. J. M. Blobaum, M. A. Wall, and A. J. Schwartz, J. Alloys Compd. **444-445**, 230 (2007).
4) Y. Imai, M. Izumiyama, and K. Sasaki, Sci. Rep. Res. Inst. Tohoku Univ. A **18**, 39 (1966).
5) J. J. Rechtien and R. D. Nelson, Metall. Trans. A **4**, 2755 (1973).
6) P. Deloffre, J. L. Truffier, and A. Falanga, J. Alloys Compd. **271-273**, 370 (1998).
7) K. J. M. Blobaum, C. R. Krenn, M. A. Wall, T. B. Massalski, and A. J. Schwartz, Acta Mater. **54**, 4001 (2006).
8) J. R. Jeffries, K. J. M. Blobaum, M. A. Wall, and A. J. Schwartz, Acta Mater. **57**, 1831 (2009).
9) J. R. Jeffries, K. J. M. Blobaum, M. A. Wall, and A. J. Schwartz, Phys. Rev. B **80**, 094107 (2009).
10) T. Lookman, A. Saxena, and R. C. Albers, Phys. Rev. Lett. **100**, 145504 (2008).
11) V. Klosek, J. C. Griveau, P. Faure, C. Genestier, N. Baclet, and. F. Wastin, J. Phys.: Condens. Matter **20**, 275217 (2008).
12) A. J. Schwartz, H. Cynn, K. J. M. Blobaum, M. A. Wall, K. T. Moore, W. J. Evans, D. L. Farber, J. R. Jeffries, and T. B. Massalski, Prog. Mater. Sci. **54**, 909 (2009).
13) J. R. Jeffries, K. J. M. Blobaum, M. A. Wall, and A. J. Schwartz, J. Nucl. Mater. **384**, 222 (2009).
14) A. Hammersley, S. Svensson, M. Hanfland, A. Fitch, and D. Hausermann, High Press. Res. **14**, 235 (1996).
15) C. Lawson, B. Martinez, J. A. Roberts, B. I. Bennett, and J. W. Richardson, Phil. Mag. B **80**, 53 (2000).
16) M. I. Baskes, A. C. Lawson, and S. M. Valone, Phys. Rev. B **72**, 014129 (2005).
17) K. T. Moore, C. R. Krenn, M. A. Wall, and A. J. Schwartz, Metall. Mater. Trans. A **38A**, 212 (2007).
18) A. N. Kolmogorov, Izv. Akad. Nauk. SSR **3**, 355 (1937).
19) M. Avrami, J. Chem. Phys. **7**, 1103 (1939).
20) M. Avrami, J. Chem. Phys. **8**, 212 (1940).

21) M. Avrami, J. Chem. Phys. **9**, 177 (1941).
22) W. A. Johnson and R. F. Mehl, Trans. Am. Inst. Min. Metall. Eng. **135**, 416 (1939).
23) Ravat, C. Platteau, G. Texier, B. Oudot, and F. Delaunay, J. Nucl. Mater. **393**, 418 (2009).